Effects of 21st Century Climate Change on the Amazon Rainforest

Kerry H. Cook and Edward K. Vizy

Cornell University

Accepted for Journal of Climate

June 2007

ABSTRACT

A regional atmospheric model with 60 km resolution is asynchronously coupled with a potential vegetation model to study the implications of 21st century climate change for the tropical and subtropical climate and vegetation of South America. The coupled model produces an accurate simulation of the present day climate and vegetation. Future climate is simulated by increasing atmospheric CO_2 levels to 757 ppmv and imposing lateral and surface boundary conditions derived from a GCM simulation for 2081-2100 from the Canadian Climate Center GCM.

The coupled regional model simulation projects a 70% reduction in the extent of the Amazon rainforest by the end of the 21st century, and a large eastward expansion of the caatinga vegetation that is prominent the Nordeste region of Brazil today. These changes in vegetation are related to reductions in annual mean rainfall and a modification of the seasonal cycle that are associated with a weakening of tropical circulation systems.

1. Introduction

The response of tropical forests to climate change, including the role they may play in determining the structure and magnitude of that change, is not yet understood. But there is great concern for the future of the world's tropical forests. In addition to their aesthetic value, tropical forests are a treasure trove of biodiversity for future medical applications, and they play important roles in determining climate and regulating the global carbon budget.

Investigations of the future of the tropical and subtropical South American climate and vegetation contain significant uncertainty. One reason is the complexity of the system, in which land surface processes are tightly coupled to the atmospheric hydrodynamics. Another reason is that the climate has a highly regional character, and the adjacent Andean topography is so steep it cannot be resolved properly even with a climate model using 10 km resolution.

However, there are indications that the Amazon rainforest may suffer greatly as a result of global warming. For example, Scholze et al. (2006) use model projections of the 21st century from 16 coupled atmosphere/ocean GCMs to drive a dynamic vegetation model, with the goal of identifying ecosystems around the world that may be vulnerable to climate change. The Amazon basin is identified as a region at high risk for extensive forest loss.

Increasing our confidence in predictions of a possible die back in the Amazon rainforest vegetation would strengthen the ability of governments to act. When independent and various techniques are applied to the problem and generate similar results, that confidence is bolstered. In this study, changes in tropical and subtropical

South American climate and vegetation that may occur by the end of the 21st century (2080-2100) due to global warming are simulated using a regional climate model (RCM) constrained by a GCM and asynchronously coupled with a potential vegetation model (PVM). The GCM output provides large-scale changes in circulation and SSTs for future climate, and the RCM is used to evaluate the implications of these changes for regional South American climate and vegetation. The RCM produces a more accurate representation of the present day South American climate than a GCM and provides regional information needed for assessing impacts.

The paper is focused on understanding how climate change due to increasing levels of greenhouse gases in the atmosphere may effect the Amazon vegetation. Human influence on vegetation, including the ongoing clearing of rainforest vegetation, is not taken into account.

In the following section, previous work on predicting the future of Amazon basin climate and vegetation is reviewed. The modeling tools used in this study are described in section 3. In section 4, we explore various approaches for using regional models to study future climate, and validate the coupled model simulation of South American climate and vegetation. Results are reported in section 5, and conclusions and implications are discussed in section 6.

2. Background

Simulating South American climate is a challenge for coupled atmosphere/ocean GCMs. The Andes topography, which is known to be an important determinant of the continental climate, is so steep that the elevation of the surface is artificially lowered by 2

km or more at typical GCM resolutions (Lenters and Cook 1995). This problem is usually addressed in models by adopting envelope topography, which preserves the volume of the topography so it produces reasonable planetary-scale perturbations of the flow. But this does not serve the regional representation of temperature and, especially, precipitation on the continent well.

Vera et al. (2006) evaluated the ability of the current generation of coupled GCM to reproduce seasonal mean precipitation over South America. While most of the models reproduce reasonable seasonal variations, except in the SACZ region, rainfall rates are quantitatively inaccurate over the Amazon basin, making them inadequate for hydrological studies and for coupling with vegetation models.

There is no consensus in the literature about how climate may change in tropical South America in the coming century due to greenhouse gas increases. Giorgi et al. (2001) examined output from 18 coupled atmosphere/ocean models under two future climate change scenarios and did not identify a consistent signal over South America within the models examined. In the current generation of coupled GCM simulations of the 21st century, i.e., those produced for the 4th Assessment Report of the Intergovernmental Panel on Climate Change (IPCC), Li et al. (2006) also found no agreement in how the climate of the Amazon basin may change in these models, with 5 of the 11 simulations examined producing a wetter climate, 3 a drier climate, and 3 no change. But a higher resolution simulation by Coppola and Giorgi (2005), using a finite-element GCM resolving 1° latitude and 1.35° longitude, simulated statistically significant annual mean precipitation decreases over the Amazon basin for 2071-2100 under relatively severe (but not unreasonable) greenhouse gas forcing. Finally, Rojas et al.

(2006) examine the global warming signal in 6 coupled AR4 GCMs, and find that the majority simulate a longer dry season in tropical South America, as part of an increase in the amplitude of the seasonal cycle of precipitation.

Coupling between the land surface and the atmosphere may complicate the effort to properly simulating the Amazon basin climate. The recycling of precipitation is thought to be important, and an accurate representation of the partitioning between sensible and latent heat fluxes depends on the treatment of evapotranspiration (Xue et al. 2006).

One application of vegetation models is coupling with atmospheric models to permit the biome to change in a simulation. Two types of vegetation models are in use. Equilibrium, or potential, vegetation models (PVMs; e.g., Claussen 1994) determine vegetation distributions that are consistent with a given climate. The time that nature would require to equilibrate vegetation to a changed climate is neglected in this equilibrium approach. Dynamic vegetation models (DVMs) are fully interactive and influence the exchange of moisture, heat, and momentum between the atmosphere and the land surface every model time step (e.g., Costa and Foley 2000). The development of DVMs, and their coupling with GCMs, is an area of ongoing research. Current versions of these models do not reproduce current vegetation distributions accurately (e.g., Cox et al. 2004, Bonan and Levis 2006), but have the potential for including important interactions among climate subsystems more completely.

Scholze et al. (2006) use output from various coupled GCM simulations, binned into three levels according to the degree of global warming simulated, to drive a DVM and calculate the probability of critical change in global ecosystems between 1961-1990

and 2071-2100. Tropical South America emerges from this analysis as a region at high risk for the conversion of significant amounts of forest to nonforested areas.

Since global warming is underway, observational analyses may also be relevant for indicating the possibility of significant climate change in the Amazon and Nordeste regions. Costa and Foley (1999) detected a decrease in the moisture transported into the Amazon basin in the NCEP/NCAR reanalysis, but Malhi and Wright (2004) found no trend in station-based precipitation data from the Amazon basin in the late 20th century.

Because of the shortcomings of various approaches to prediction, there is great value in applying various methodologies to the problem. In this study we contribute to an understanding about how the climate and vegetation of tropical South America may change in the future by applying a regional atmosphere-only climate model (RCM) coupled with a PVM to the problem. The strengths of this approach are the relatively high resolution of the model and the good simulation of the present day climate and vegetation distributions – better than what has emerged from GCM studies. But because the coupled atmosphere/vegetation model does not include an interactive ocean, the simulation depends on output from a coupled atmosphere/ocean GCM to provide lateral boundary conditions and SSTs.

3. RCM/PVM model description

The RCM is the Pennsylvania State University/National Center for Atmospheric Research (PSU/NCAR) MM5 (v3.6) model (Grell et al. 1994) adapted for climate studies in the tropics.

Our previous experience using this RCM over South America (Vizy and Cook 2005, 2007; Cook and Vizy 2006) guides choices in the physical parameterizations that yield a state-of-the-art simulation of the South American climate. These include the Kain-Fritsch cumulus parameterization (Kain and Fritsch 1993), the shallow cumulus parameterization of Grell et al. (1994), and the MRF planetary boundary layer scheme (Hong and Pan 1996). Cloud ice is included using the "simple ice" scheme developed by Dudhia (1989).

Lateral and surface boundary conditions (as specified below) are updated every 12-hours during integrations that are 382 days long (a full year plus 17 days for spin up). Horizontal resolution of 60 km is used, with 24 vertical σ-levels, and the time step is 1 minute.

The regional model domain includes the entire continent (from 55°S to 12°N, and 28°W to 92°W). This exceptionally large domain allows SSTs near the continent to influence climate within the regional model, and places the lateral boundaries almost exclusively over the oceans. This is important because we want to insert boundary conditions from the GCM that reflect large-scale conditions. In this simulation design, we are relying on the coupled GCM to provide changes in the large-scale climate, particularly the circulation. Placing the lateral boundaries off the continent aids in this effort because the continental surface introduces regional space scales into the system.

The Noah land surface model parameterization (LSM; Chen and Dudhia 2001) couples the land surface to the atmosphere. Given information about the "landuse", i.e., vegetation type, the LSM calculates moisture and temperature in four soil layers, canopy

moisture, water-equivalent snow depth, and surface and underground run-off accumulations.

Coupling the PVM to the RCM allows the vegetation type to change. The PVM takes climate conditions as input and diagnoses the vegetation distribution that is consistent, and in equilibrium, with that climate state. Differences between the vegetation from a PVM and observations can result when the vegetation is not in equilibrium with the climate, and when factors other than climate influence vegetation (e.g., human intervention, soil type). Climate is the primary (non-anthropogenic) determinant of vegetation distributions except on small space scales (Woodward 1987).

The PVM of Oyama and Nobre (2004) at the Centro de Previsao de Tempo e Estudios Climaticos (CPTEC) is used. The CPTEC PVM is similar in structure to other PVMs in use, such as the BIOME model and its offspring (Prentice et al. 1992), but it does not account for ecological competition between plants. The CPTEC PVM, however, validates particularly well over South America, at least in part because it includes a consideration of seasonality in determining biome type that improves the model performance for tropical forests.

Vegetation type is determined by considering 5 parameters, 3 related to temperature and 2 related to moisture. The temperature variables are the mean temperature of the coldest month (T_C), and the number of growing degree days using two bases, namely, 0°C and 5°C. The moisture variables are the wetness index, H, and the seasonality index, D. H is defined by

$$H = \frac{\sum_{i=1}^{12} g_i E_i}{\sum_{i=1}^{12} g_i E_{max,i}}, \qquad (1)$$

where E is the evapotranspiration rate, E_{max} is a maximum allowed evapotranspiration rate, and the summation is over months for regions in which the soil is not frozen. The factor, g, is zero for frozen ground, and 1 otherwise. E is evaluated using the Penman-Monteith equation [see, for example, Eq. 6 in Oyama and Nobre (2004)].

The seasonality index is defined as

$$D = 1 - \frac{\sum_{i=1}^{12} F\left[0.5 - w_i\right]}{6}, \tag{2}$$

where w_i is the fractional soil saturation, i.e., the ratio of the soil moisture to the soil's water holding capacity. $F\left[0.5 - w_i\right] = 0.5 - w_i$ when $\left(0.5 - w_i\right) \geq 0$, and zero otherwise. For any given month, if $w_i > 0.5$, i.e., for soil saturation values of 50% or greater, $F\left[0.5 - w_i\right] \equiv 0$. So larger values of D result for wetter conditions over the year, and if the soil is at least 50% saturated every month, then D = 1.

In order to use the CPTEC PVM with MM5, the vegetation categories used by Oyama and Nobre (2004) were translated into the USGS categories. This is a one-to-one renaming. "Tropical forest" is renamed "evergreen broadleaf forest" in the USGS nomenclature, and "caatinga" is renamed "mixed shrubland/grassland". (Caatinga refers to the semi-arid vegetation that covers more than 10% of the surface area of Brazil, primarily in the drought-prone Nordeste region.) Also, "desert" is called "barren or sparsely vegetated", and "semi-desert" is "shrubland" in the USGS terminology. The "savanna" and "grasslands" designations are the same.

The growing degree day factors are effective for distinguishing among colder climates, but do not come into play for tropical biomes in general. When $T_C > 6°C$, the biome will be one of four choices - tropical forest, savanna, shrublands, or grasslands –

depending on the moisture variables. If the climate is quite dry, with $H < 0.28$, the PVM will evaluate the vegetation as semidesert (shrubland). A somewhat wetter climate, with $0.28 \leq H < 0.55$ and $D < 0.46$ will be designated "mixed shrubland/grassland" (caatinga).

Oyama and Nobre (2004) require $T_C \geq 11°C$ for the rainforest vegetation to optimize the model for global application (Oyama, personal communication), but here we use $T_C \geq 15°C$ as in Prentice et al. (1992) because this produces a more realistic result over South America. In addition, tropical forests require wet annual conditions ($H \geq 0.80$) and a short dry season ($D \geq 0.91$). When moisture levels are intermediate, with $0.55 \leq H < 0.80$ and $0.46 \leq D < 0.91$, T_C is used to distinguish between grasslands ($6°C \leq T_C < 14°C$) and savanna ($14°C \leq T_C$).

The PVM and the RCM are coupled asynchronously, as illustrated in Figure 1. The RCM is first run to generate an annual climatology under specified climate forcing factors such as atmospheric CO_2, SSTs, and lateral boundary conditions, and a first-guess vegetation distribution. Then temperature and moisture parameters derived from the resulting climate state are used to produce a new vegetation distribution using the PVM, and the RCM is rerun with the new vegetation prescribed. The process continues until the vegetation distribution stabilizes. This stabilization may involve small oscillations in biome type, but no trends. In this way, the vegetation distribution can evolve in response to the modeled climate, and changes in vegetation can influence the final climate state.

4. Simulation design and model validation

There is no standardized methodology for studying future climate using regional climate models. The problem is the same as for paleoclimate studies – how should one constrain the lateral boundaries, and what surface boundary conditions should be used (e.g., Vizy and Cook 2005; Cook and Vizy 2006)? But there is great motivation for using regional models for climate change studies because they can provide regionally-specific information useful for developing strategies to reduce climate change impacts. With these ideas in mind, we tried a variety of approaches to simulate the climate of 2081-2100, as discussed below.

The first step is to produce a good simulation of the present day climate of South America. Two attempts were made with the RCM uncoupled from the PVM, with the observed vegetation distribution (Fig. 3a) specified. In one attempt, labeled "Present_Reanalysis" in Table 1, surface, initial, and lateral boundary conditions are specified using the NCEP/NCAR reanalysis climatology for 1981-2000, including observed SSTs. In another, these conditions are taken from a GCM.

To choose a GCM to provide boundary conditions for the RCM, we evaluated 20th century integrations of 21 coupled ocean/atmosphere GCMs over South America to identify the models which more accurately capture key circulation features within our domain, e.g., the Bolivian high, ITCZ, SACZ, and the South American low level jet. The coupled GCMs evaluated were from modeling groups that contributed to the 4th Assessment Report of the IPCC. We also evaluated the rainfall distribution during the entire annual cycle, and consulted the analysis of Dai (2006) who evaluated the tropical precipitation climatology and its variability in 18 of the IPCC coupled GCMs. These

considerations led to three GCMs, namely, CGCM3.1 from the Canadian Centre for Climate Modelling and Analysis (CCCMA); MIROC3.2 from the Center for Climate System Research (The University of Tokyo), National Institute for Environmental Studies, and Frontier Research Center for Global Change (JAMSTEC); and CGCM2.3.2 from the Meteorological Research Institute (MRI). From these, we chose to use output from CCCMA CGCM3.1 to use with the RCM. The lateral boundary conditions from this model were examined to be sure that small-scale structure generated in the GCM simulation was not being introduced on the boundaries, since the goal is to use the GCM to communicate changes in large-scale conditions into the RCM domain.

Annual mean precipitation climatologies from observations, the CCCMA 20th century integration, the RCM constrained by CCCMA boundary conditions (Present_CCC in Table 1), and the RCM constrained by the reanalysis (Present_Reanalysis in Table 1) are displayed in Figure 2. [Note that Fig. 2a is a blend of satellite/gauge observations plotted over the oceans (Xie and Arkin 1997), and a higher resolution rain gauge data set over land (New et al. 2000)]. The CCCMA 20th century integration captures a precipitation maximum over the Amazon basin, and higher rainfall to the southwest in the Andes foothills, similar to the observations, but the relatively dry region between the two maxima is exaggerated. The Pacific ITCZ is well simulated, but the Atlantic ITCZ is weak and misplaced. The SACZ is not well defined, the dry region of the Nordeste is not resolved. The northeastern coast is too dry. Despite these differences from the observations, this is one of the best simulations of annual mean precipitation over South America among the AR4 coupled models. For example, if one averages South American precipitation simulations in the AR4 coupled models' 20th

century simulations, there is not a precipitation maximum located over the Amazon basin (Menendez 2005).

In the two RCM simulations (Figs. 2c and d), rainfall rates are very high over the oceans, perhaps partly because the resolution of the CPC observations is low (2.5°, or ~ 250 km) compared with that of the RCM (60 km). Over the continent, Present_Reanalysis provides a significantly better representation than Present_CCC. In particular, the Amazon precipitation maximum is better formed in Present_Reanalysis, and the Nordeste is appropriately dry.

The PVM provides a powerful validation tool for the regional climate model because it can be used to translate a simulated climate state into a vegetation distribution that can be compared directly with the observed vegetation distribution. Climate parameters from the two present day simulations described above and the CCCMA GCM output are used to drive the PVM and generate the vegetation distribution in equilibrium with the modeled climate. This synthesizes the model validation in terms of the ability of the modeled climate to support the observed vegetation.

Figure 3b shows the simulated PVM vegetation distribution that is consistent with the CCCMA GCM climatology for 1981-2000. Simulated vegetation distributions from the Present_CCC and Present_Reanalysis climatologies are displayed in Figs. 3 c and d, respectively. It is clear that the Present_Reanalysis climatology produces a realistic vegetation distribution, while the vegetation distributions consistent with the CCCMA and Present_CCC climatologies have significant disagreements with the observations. Note that the greatest difference between the observed vegetation and that modeled in the

Present_Reanalysis integration is the elimination of cropland, which is not accounted for in the PVM model algorithm.

The quality of the present day simulations shown above strongly motivates the choice of boundary conditions from the reanalysis for the "present day control" simulation. This control simulation, called "Present_Coupled" in Table 1, is performed with the vegetation asynchronously coupled, as outline in Figure 1. Only minor changes in the climate and the vegetation distribution result from this coupling, and only one iteration is performed. The vegetation distribution for the Present_Coupled simulation is shown in Figure 4a, with political boundaries added.

GCM output is required for the 21st century RCM simulation, as is a choice in emissions scenarios for the future. We use the climatology for 2081-2100 from the CCCMA GCM forced by the A2 emissions scenario, which assumes that CO_2 emissions continue to grow at essentially the present day rate throughout the 21st century, and set the CO_2 concentration within the RCM to 757 ppmv, which is the 2081-2100 average for this scenario.

To be consistent with the decision to use the reanalysis for the RCM boundary conditions in the present day simulation, lateral and surface boundary conditions for future simulations are constructed by adding differences between the 2081-2100 and 1981-2000 means from the CCCMA integrations to the 1981-2000 reanalysis values and observed SSTs. (If the full CCCMA values from the 2081-2100 climatology are used on the boundaries, differences from the present day simulation would be a combination of differences due to climate change and errors in the CCCMA present day climatology.) Three iterations are performed to coupled the PVM and RCM, since the coupled system

quickly converges to a stable vegetation distribution, and the simulation is referred to as Future_Coupled in Table 1.

5. Results

a. Simulated changes in South American climate and vegetation

The vegetation distribution from the coupled RCM/PVM simulation for 2081-2100 (denoted Future_Coupled in Table 1) is shown in Figure 4b. Compared with the present day simulation (Fig. 4a), the areal extent of the Amazon rainforest is reduced by 69%. A total loss of rainforest vegetation in the central and southern Amazon basin is simulated. Bolivia, Paraguay, and Argentina lose all of their rainforest vegetation, and Brazil and Peru lose most of it. The surviving rain forest is concentrated near the equator, with the rainforest extent in Columbia essentially maintained. Along the northern coast, Venezuela and French Guiana suffer relatively small reductions in rainforest extent, while the loss in Guyana and Surinam is 30-50%.

Much of the rainforest in the central Amazon north of about 15°S is replaced by savanna vegetation, but in southern Bolivia, northern Paraguay, and southern Brazil, grasslands take the place of the rainforest in the 2081-2100 simulation. (Some of this area is not rainforest today, having been replaced by cropland as seen in Fig. 3a, but the present day climate in that region would support rainforest.) East of about 52°W over a large portion of Brazil, present day savanna is replaced by shrubland as the caatinga vegetation of the Nordeste region spreads westward and southward. In the heart of this region (from about 5°S-12°S, centered around 40°W), present day caatinga vegetation is replaced by barren land.

To understand what features of the changed climate are related to these differences in vegetation, the criteria for each biome type specified in the PVM are examined. As discussed in section 3b, one climate criterion for the existence of a tropical forest is that the mean temperature of the coldest month must exceed 15°C ($T_C \geq$ 15°C). In the present day simulation, this criterion is met everywhere north of about 25°S, except in the high Andes (not shown). In the 2081-2100 simulation, surface temperatures increase by 2-4°C through most of this region in winter, so the T_C criterion is not related to the rainforest reduction.

The demise of the rainforest is related to the moisture parameters, H and D (see section 3b). In Figures 5a and b, the shaded regions are those in which there is insufficient annual moisture ($H \leq 0.80$; Eq. 1) to maintain the rain forest in the 1981-2000 and 2081-2100 simulations, respectively. In the present day simulation, annual precipitation rates are too low for rain forest vegetation east of about 52°W from roughly 16°S to 4°S, in the Andes Mountains and along the west coast, and in northern Venezuela and parts of Columbia. In the simulation for 2081-2100 (Fig. 5b), all of the South American continent between approximately 20°S and 3°S fails to pass the wetness condition for rainforest vegetation, with the exception of a few small isolated regions (refugia). Dry patches also develop between the equator and 5°N.

The role of the seasonality parameter, D, in setting the rainforest boundary in the present day simulated climate is shown in Fig. 5c, in which the shading denotes areas in which $D < 0.91$ (Eq. 2), i.e., in which the climate cannot support rainforest vegetation because the dry season is too long. The gray contour repeats the edge of the shaded region in Fig. 5a. The similarity of the D and H parameters indicates that the changes in

seasonality captured by the D parameter, i.e., increasing the length of the dry season, are in large part responsible for the annual mean drying represented by H. Since the rainforest criteria on H and D must both be met for rainforest vegetation, Fig. 5c indicates that the southern boundary of the rainforest near 15°S in the eastern Amazon is being controlled by annual precipitation rates.

Shading in Fig.5d denotes regions in which the seasonality parameter excludes the presence of rainforest in the 2081-2100 simulation and, again, the gray line repeats the boundary from the wetness parameter, H, in Fig. 5b. The changed seasonality of rainfall in the 2081-2100 simulation removes the refugia and expands the area of the savanna vegetation that replaces rainforest in Surinam and Guyana.

The expansion of the caatinga in the 2081-2100 coupled RCM/PVM simulation is also related to changes in moisture regimes. Shading in Figures 6a and b designates areas in which the wetness criterion for caatinga vegetation ($0.28 \leq H < 0.55$; Eq. 1) is met in the 1981-2000 and 2081-2100 simulations, respectively. Figures 6c and d display the caatinga boundaries imposed by the long dry season, with $D < 0.46$. In the present day simulation, the extent of the caatinga vegetation is largely controlled by the seasonality parameter, since the shading in 6c is contained within the contour and both criteria must be met. In the future simulation, the appearance of shaded regions outside of the contour line in the continental interior indicates that the lengthening of the dry season alone would support even more caatinga vegetation, but annual rainfall amounts are too large. The seasonality parameter constrains the northward caatinga expansion somewhat.

Figures 5 and 6 motivate an examination of the differences in precipitation between the present day and future simulations, including its seasonality. Figure 7 shows

differences in the annual mean precipitation for the future minus the control simulation. Precipitation rates decrease by more than 4 mm/day over large portions of the domain, with decreases greater than 10 mm/day in southeastern Brazil and the SACZ, which weakens and shifts to the southwest. Close to the equator, annual mean rainfall increases by more than 2 mm/day in the central and eastern parts of the continent, and along the eastern slopes of the Andes. There is pronounced drying of the ITCZ over both the Atlantic and Pacific close to the continent, and drying on the adjacent land surfaces. In the Andes, the precipitation signal adopts the space scale of the topography, which is finer than the space scales of the precipitation differences over the rest of the continent. Some high altitude regions are wetter, and some are drier, and Vizy and Cook (2007) find that such structure is closely related to not only the topography (as resolved by the model) but also to the specification of land surface conditions (which are not well known in this region).

Precipitation averages are calculated for each month within the six regions denoted by the boxes in Fig. 7, and displayed in Figure 8. These regions were chosen to capture the vegetation changes plotted in Fig. 4, but with reference to the differences in annual precipitation shown in Fig. 7. Regions A and B represent the equatorial western and central Amazon, respectively, in which the rainforest persists through the 21st century (Fig. 4) despite the fact that their precipitation anomalies have opposite signs (Fig. 7). In Region C, which covers a large part of the Southern Hemisphere central Amazon in the present day climate, rainforest is replaced by savanna by the end of the century. The same is true in Region D, in the equatorial eastern Amazon, while in Region E, only a

few degrees of latitude farther north, the rainforest is preserved despite annual mean drying. Region F captures the westward expansion of the caatinga.

In Regions A and B, precipitation rates simulated for 2081-2100 during the rainy season are equal to or greater than for 1981-2000, but the dry season is longer due to a delay in the onset of the rainy season. In Region A, the delay in the onset is accompanied by an early end to the rainy season, and the dry signal dominates in the annual mean. But these changes in the annual mean precipitation, and its seasonal signature, are not sufficient to shift either the H or D parameters of the PVM into a different biome category.

Similar to Regions A and B, Region C experiences an increase in the length of the dry season. But the increase is more pronounced than in the two equatorial regions, and there is no compensating increase in rainfall during the rainy season. As a result, 2081-2100 simulated annual rainfall totals are approximately 45% lower than in the present day simulation and the PVM specifies savanna vegetation.

Regions D and E both have negative annual mean precipitation anomalies (Fig. 7), but the rainforest vegetation is eliminated only in Region D. According to Fig. 5, the seasonality criterion, D, plays a critical role in the rainforest demise in Region D. In these two Northern Hemisphere regions, rainfall has less pronounced seasonal variations than in the Regional A, B, and C. There is a tendency for maximum rainfall during the transition seasons in the present day simulation (and in the observations), but with substantial precipitation maintained through the other months as well. In the 2081-2100 simulation, however, Region D experiences a 70% reduction in rainfall for the entire second half of the calendar year. In Region E, there are similar reductions (~ 68%) in

rainfall, but for a somewhat shorter time since the precipitation recovers in October and November, instead of in December and January as in Region D. In Region D, the dry season becomes too long to support rainforest vegetation in the future simulation.

In the 2081-2100 simulation, the dry shrublands of today's climate in the Nordeste spread significantly eastward, into Region F, for example. This change in vegetation is associated with changes in both the annual mean precipitation and its seasonality according to Fig. 6. This result is supported by Fig. 8f, which shows that the dry season in Region F lengthens significantly, mainly due to a delayed onset of the rainy season in austral spring, and that the rainy season precipitation is reduced by more than a factor of two.

To further understand the response of the precipitation and vegetation fields, the changes in the hydrodynamical fields that accompany them are examined.

Once the monsoon rainfall begins, simulated precipitation rates in the future simulation are comparable to those in the present day in each region except the central equatorial Amazon (Region B) and the eastern Amazon (Region F). In Region B, rainfall rates are greater in the future than in the present day, and in Region F they are smaller. During these months in the 1981-2000 simulation, represented by January in Figure 9a, northeasterly flow from the equatorial Atlantic advects moisture onto the continent between about 15°S and 10°N. Convergence of this flow supports the Amazon precipitation maximum (Fig. 2). Some of this moisture is channeled along the eastern flank of the Andes into the northwesterly South America low-level jet (SALLJ). South of about 15°S, the jet forms part of the cyclonic circulation around the Chaco low (centered near 25°S and 60°W). Convergence between the northwesterly flow north and east of the

Chaco low and the easterly flow onto the continent (5°S- 20°S) forms the continental base of the SACZ and supports summer rainfall in the eastern Amazon (Lenters and Cook 1995).

In the warmer climate of the 2081-2100 simulation for January (Fig. 9b), geopotential heights are greater throughout the domain, and geopotential height gradients are smaller. In particular, the Chaco low is significantly weaker, and the anomalous flow (Fig. 9c) is anticyclonic. The weaker SALLJ is associated with enhanced moisture convergence and rainfall in the central equatorial Amazon (Region B), and reduced moisture convergence and rainfall in the eastern Amazon (Region F).

The weakened state of the continental circulation in the 2081-2100 simulation persists through austral fall, the months of strongest precipitation in the Nordeste in today's climate. In the present day climate (as observed and simulated), the Chaco low is still in place in March (Fig. 9d), and doesn't break down until May (not shown). But in the 2081-2100 simulation, the Chaco low collapses in March. As a result, moisture advection by the SALLJ is weaker than in the present day simulation, and it proceeds south rather than being directed eastward to converge with the onshore flow of moisture (Fig. 9e). The resulting northward moisture advection anomaly (Fig. 9f) enhances precipitation in the central and western Amazon (Regions A and B; see Figs. 8a and b). Dry conditions in the Nordeste and throughout the eastern Amazon accompany this early demise of the Chaco low and the attendant weakening of the northwesterly flow. In the eastern Amazon and the Nordeste, precipitation rates decline below summer values at a time when the present day climate experiences a precipitation maximum (Fig. 8f).

In austral spring, modeled rainfall rates in the 2081-2100 simulation are lower than in the 1981-2000 simulation everywhere on the continent, reflecting a 1-3 month delay in the beginning of the rainy season. In contrast to the summer (Fig. 9), there is a large difference in the flow onto the continent from the tropical Atlantic in the late winter and early spring. In the 1981-2000 simulation for August (Fig. 10a), a closed thermal low has developed along the equator in the western Amazon, and moisture is being advected down the geopotential height gradient to support the beginning of the monsoon season. In the 2081-2100 August simulation (Fig. 10b), the low has not yet formed and the moisture transport runs parallel to the northeastern coast of South America. The anomalous moisture advection is directed off the continent (Fig. 10c).

Rainfall rates strengthen over the central Amazon basin (Figs. 8a and b) during September for the present day climate, as the South American monsoon begins to intensify. The thermal low is centered in the Southern Hemisphere, near 10°S, and the moist flow from the tropical Atlantic penetrates across the equator (Fig. 10d). In the 2081-2100 September simulation (Fig. 10e), the thermal low is finally in place on the equator, similar to the August case for the present day (Fig. 10a), and the flow from the tropical Atlantic has turned to begin the transport of moisture onto the continent. Across the tropical regions on the continent, the anomalous flow is southerly (Fig. 10f), indicating the reduction in cross equatorial flow during September.

In summary, differences in the rainfall regimes across South America in the simulation of the end of the 21st century are related to two regional circulation features. One is the weaker and shorter-lived Chaco low, and the other is a later development of the summer thermal low in the equatorial Amazon. These differences overlay a

background regional circulation that is weaker, e.g., with higher low-level geopotential heights throughout the model domain.

b. Relationship of the regional South America climate change to global-scale warming

Three additional simulations for 2081-2100 were run to identify the forcing factor or factors that lead to the drying and vegetation changes simulated for the future in the regional model. One simulation is identical to Present_Reanalysis (see Table 1) except atmospheric CO_2 concentrations within the regional model are increased from 330 ppmv to 757 ppmv. This simulation is named "CO_2-Alone" in Table 1. In another simulation, "SST-Alone" in Table 1, only future SST forcing from the CCC coupled GCM simulation is applied. Finally, the role of the changed lateral boundary conditions is isolated in the "Lateral-Alone" simulation described in Table 1.

The drying and dieback of the Amazon vegetation simulated in the Future_Coupled simulation do not occur in the CO_2-alone and SST-alone simulations. In fact, there is a slight expansion of the rainforest to the south and east in these simulations (not shown). In contrast, when the future lateral boundary conditions from the CCCMA simulation for 2081-2100 are applied to the regional model in the lateral-alone simulation, the response is very similar to that of Future_Coupled. So the lateral boundary conditions on temperature, winds, and atmospheric moisture, i.e., changes in the large-scale hydrodynamics, force the regional changes in climate and vegetation.

This raises the issue of whether or not the results are highly dependent on the particular GCM used to generate future lateral boundary conditions. The lateral boundary conditions from the CCCMA simulation imposed an overall weakening of the

large-scale tropical circulation – the Walker circulation in particular. The regional model responds with a weakening of regional scale circulation features and precipitation, as discussed above, that is compatible with the weakening of the large-scale circulation. Confidence in these results is strengthened by noting that a similar weakening of large-scale tropical circulations – particularly Walker circulations - is produced in *all* of the AR4 model simulations of the 21st century (Vecchi and Soden 2007). In addition, a theoretical understanding of why large-scale tropical circulations should weaken with global warming has been advanced (e.g., Betts and Ridgway 1989, Held and Soden 2006). Recent observational analyses indicate a weakening trend for the Walker circulation, especially in the Pacific (Tanaka et al. 2004; Vecchi et al. 2006, Zhang and Song 2006), but it some studies suggest a strengthening of the Hadley circulation, especially during boreal winter (Chen et al. 2002; Tanaka et al. 2004; Mitas and Clement 2005).

These factors suggest that the dependence on the GCM chosen for the lateral boundary conditions in the regional simulation may not be strong. If the simulations with future climate conditions applied individually had demonstrated that SST forcing was responsible for the changed South American climate, we might have less confidence in the independence of the results from the lateral boundary conditions imposed because the AR4 coupled GCMs have a much greater range in behavior of SSTs in simulations of the future.

c. Role of vegetation changes

The influence of vegetation on climate is accounted for by the inclusion of the NOAH LSM within the regional climate model. We find that simulations of South America without the LSM do not produce an accurate climate, indicating the importance of vegetation for determining climate over South America. However, vegetation type cannot change in response to climate in the NOAH LSM. The asynchronous coupling with the PVM provides this function, and an opportunity to evaluate the influence of feedbacks from vegetation changes on climate.

The changes in climate that result from the vegetation feedback include added warming of about 0.5 K in the Amazon basin, and of about 2 K in the Nordeste (not shown). This is consistent with simulations of a different design by Feddema et al. (2005), in which an imposed expansion of cropland in the Amazon in simulations of future climate resulted in added warming of the land surface. But, as discussed above, the vegetation is not very sensitive to the added warming.

The asynchronous coupling of the RCM and PVM illustrated in Fig.1 produces a series of vegetation states. Figure 11a shows the "1st iteration vegetation", and Fig. 11b is the "2nd iteration vegetation" for the future climate simulation. The stabilized vegetation distribution, produced by three iterations, was displayed in Fig. 4b. The third iteration was the final one because trends in vegetation distributions were no longer present after the second iteration.

Most of the final vegetation response is produced in the first iteration (compare Figs. 11a and 4b). This is consistent with the results of Cox et al. (2004), who found that the primary cause of the die-back in Amazon vegetation was due to climate forcing and not vegetation feedbacks in their coupled GCM/PVM study.

But there are some important regional differences that result from the feedback of vegetation on climate. The vegetation distribution from the 1st iteration (Fig. 11a) sustains rainforest vegetation south of 5°S, mixed with savanna across western Brazil and a large portion of Peru, and far northern Peru is covered solidly with rainforest vegetation. In the next iteration (Fig. 11b), the rainforest boundary retreats approximately 5° of latitude farther north in the western and central Amazon. The third iteration (Fig. 4b) produces no significant additional change in the southern boundary of the rainforest.

Another difference between the 1st iteration vegetation and the 2nd iteration vegetation (Figs. 11a and b, respectively) is that the caatinga extends farther west in the 2nd iteration than in the 1st, with patches of this shrubland vegetation appearing within the savanna that becomes established across central Brazil in the 2081-2100 simulation. The pattern is modified in the 3rd iteration, but the patchiness of the eastern Amazon savanna of the future climate remains.

6. Conclusions and Discussion

A regional atmospheric model with 60 km resolution is asynchronously coupled with a potential vegetation model to study the effects of 21st century climate change on the tropical and subtropical climate and vegetation of South America. Changes in vegetation due to climate change are simulated, and vegetation changes feed back to influence the climate. This approach assumes that the climate change is slow enough that the vegetation remains in equilibrium with the climate. Vegetation changes due to direct human activity, such as cutting and burning of vegetation and agricultural activity, and

perturbations to the global carbon cycle associated with vegetation changes, are not included.

The present day climate is simulated by constraining the regional model with lateral and surface boundary conditions from the NCEP/NCAR reanalysis averaged over 1981-2100. The regional model produces a representation of the present day climate that is sufficiently precise to reproduce the observed present day distribution of vegetation across the continent.

Future climate is simulated by raising CO_2 levels in the regional model to 757 ppmv, consistent with the IPCC's A2 forcing scenario for 2081-2100, and by imposing lateral and surface boundary conditions based on a GCM simulation for 2081-2100 under the same emissions scenario. The Canadian Climate Center model (CCCMA) is chosen for its relatively good representation of the large-scale tropical climate in 20th century simulations. Boundary conditions for the regional model are constructed by adding differences between the 2081-2100 and 1981-2000 means from the CCCMA integrations to the 1981-2000 reanalysis values and observed SSTs. This simulation design, including the choice of a large domain that includes the South American continent and adjacent ocean, is intended to communicate changes in the large-scale circulation into the regional modeling domain while allowing the regional model to solve for the continental-scale features of the climate change.

The coupled regional model simulation projects a 70% reduction in the extent of the Amazon rainforest by the end of the 21st century (2081-2100), and a large eastward expansion of the caatinga vegetation (mixed shrubland and grasses). Rainforest vegetation disappears entirely from Bolivia, Paraguay, and Argentina, and most of Brazil

and Peru. Rainforest in Columbia is largely maintained, as all of the surviving rain forest is concentrated close to the equator. Venezuela and French Guiana experience small reductions in rainforest extent, but the loss in Guyana and Surinam is 30-50%. North of about 15°S, the rainforest is primarily replaced by savanna vegetation. Farther south, in southern Bolivia, northern Paraguay, and southern Brazil, grasslands take over. Present day savanna is replaced by caatinga vegetation over a large portion of eastern Brazil, and some of today's caatinga converts to barren land.

A prominent role of vegetation changes feeding back to influence climate was not simulated on continental space scales, but this feedback caused an additional equatorward retreat of the rainforest by about 5° latitude in the western Amazon.

These changes in vegetation are due to reductions in annual mean rainfall and a modification of the seasonal cycle of rainfall that increases the length of the dry season over much of tropical and subtropical South America. The lengthening of the dry season in many regions is associated with a delayed onset of the monsoon circulation in austral spring, as well as the late formation and early demise of the Chaco low. The precipitation reductions are accompanied by an overall weakening of the tropical circulation within the regional modeling domain.

A weakening of the tropical circulation applied on the lateral boundaries of the regional model is identified as the forcing factor responsible for the changed future South American climate and vegetation. Since all AR4 coupled GCMs simulations under various forcing scenarios for future greenhouse gas concentrations agree that the tropical circulation will weaken (Vecchi and Soden 2007), a theoretical understanding is in place (Betts and Ridgway 1989, Held and Soden 2006), and observational analyses have

detected such a weakening of the Walker circulation in the Pacific (Vecchi et al. 2006, Zhang and Song 2006), confidence in these results – and their model independence - is strengthened.

Further confidence in this approach to simulating future climate derives from the ability of the regional model to reproduce the South American climate with sufficient accuracy so that the vegetation distribution in equilibrium with the modeled climate is very realistic. This is not the case for the current generation of coupled GCMs. Another advantage is the relatively high resolution of the regional model, which provides information about climate change on space scales that are relevant to political boundaries and, therefore, policy decisions. Finally, application of the vegetation model allows us to present the results in terms of vegetation changes in the future instead of just changes in, say, temperature and precipitation which are hard to interpret in terms of their impacts.

Acknowledgements.

We gratefully acknowledge the international modeling groups for providing their data for analysis, the Program for Climate Model Diagnosis and Intercomparison (PCMDI) for collecting and archiving the model data, the JSC/CLIVAR Working Group on Coupled Modelling (WGCM) and their Coupled Model Intercomparison Project (CMIP) and Climate Simulation Panel for organizing the model data analysis activity, and the IPCC WG1 TSU for technical support. The IPCC Data Archive at Lawrence Livermore National Laboratory is supported by the Office of Science, U.S. Department of Energy. We also greatly appreciate that M. D. Oyama and C. A. Nobre at CPTEC made their

PVM available for this application. Financial support from NASA Award NNG05GR52G made this work possible.

References

Betts, A.K., and W. Ridgway, 1989: Climatic equilibrium of the atmospheric convective boundary-layer over a tropical ocean. *J. Atmospheric. Sci*., **46**, 2621-2641.

Bonan, G.B., and S. Levis, 2006: Evaluating aspects of the community land and atmosphere models (CLM3 and CAM3) using a Dynamic Global Vegetation Model. *J. Cli*., **19**, 2290-2301.

Chen, F., and J. Dudhia, 2001: Coupling an advanced land-surface/hydrology model with the Penn State/NCAR MM5 modeling system. Part I: Model implementation and sensitivity. *Mon. Wea. Rev.*, **129**, 569-585.

Chen, J. Y., B. E. Carlson, and A. D. DelGenio, 2002: Evidence for strengthening of the tropical general circulation in the 1990s. *Science*, **295**, 838-841.

Claussen, M. 1994: Coupling global biome models with climate models. Climate Research, 4, 279-583.

Colinvaux, P. A., G. Irion, M. E. Rasanen, M. Bush, and J. A. de Mello, 2001: A paradigm to be discarded: Geological and paleoecological data falsify the Haffer & Prance refuge hypothesis of Amazonian speciation. *Amazonia – Limnologia et Oecologia Regionalis Systemae Fluminis Amazonas,* **16**, 606-646.

Cook, K.H., and E. K. Vizy, 2006a: South American climate during the Last Glacial Maximum: Delayed onset of the South American monsoon. *J. Geophy. Res. – Atmospheres*, *111*, D02110, doi:10.1029/2005JD005980.

Coppola, E., and F. Giorgi, 2005: Climate change in tropical regions from high-resolution time-slice AGCM experiments. *Quart. J. Roy. Meteorol. Soc*., **131**, 2132-3145.

Costa, M.H., and J.A. Foley, 1999: Trends in the hydrologic cycle of the Amazon basin. J. Geophys. Res. – Atmospheres, 104, 14189-14198.

Costa, M.H., and J.A. Foley, 2000: Combined effects of deforestation and doubled atmospheric CO_2 concentrations on the climate of Amazonia. J. Climate, 13, 18-34).

Cox, P.M., R.A. Betts, M. Collins, P.P. Harris, C. Huntingford, and C.D. Jones, 2004: Amazonian forest dieback under climate-carbon cycle projections for the 21st century. *Theor. and Applied Climatology*, **78**, 137-156.

Dai, A., 2006: Precipitation characteristics in eighteen coupled climate models. *J. Climate*, **19**, 4605-4630.

Feddema, J.J., K.W. Oleson, G.B. Bonan, L.O. Mearns, L.E. Buja, G.A. Meehl, and W.M. Washington, 2005: The importance of land-cover change in simulating future climates. *Science*, **310**, 1674-1678.

Foley, J.A., S. Levis, M.H. Costa, W. Cramer, and D. Pollard, 2000: Incorporating dynamic vegetation cover within global climate models. *Ecological Applications*, **10**, 1620-1632.

Giorgi, F., P.H. Whetton, R.G. Jones, J.H. Christensen, L.O. Mearns, B. Hewitson, H. von Sotrch, R. Francisco, and C. Jack, 2001: Emerging patterns of simulated regional climatic changes for the 21st century due to anthropogenic forcings. *Geophys. Res. Lett*., **28**, 3317-3320.

Grell, G. A., J. Dudhia, and D. R. Stauffer, (1994), A description of the fifth-generation Penn State/NCAR mesoscale model (MM5), NCAR Tech. Note TN-398+STR, 122 pp.

Haberle, S. G., and M. A. Maslin, 1999: Late Quaternary vegetation and climate change in the Amazon basin based on 50,000 year pollen record from the Amazon fan, ODP Site 932. *Quat. Res*., **51**, 27-38.

Held, I. M., and B. J. Soden, 2006: Robust responses of the hydrological cycle to global warming. *J. of Climate,* **19**, 5686-5699.

Hong, S.-Y., and H.-L. Pan, 1996: Nonlocal boundary layer vertical diffusion in a mediumrange forecast model, *Mon. Wea. Rev*., **124**, 2322-2339.

Kain, J. S., and J. M. Fritsch, 1993: Convective parameterization for mesoscale models: The Kain-Fritsch scheme, *The representation of cumulus convection in numerical models*, K. A. Emanuel and D. J. Raymond, Eds., Amer. Met. Soc., 246 pp.

Kastner, T. P., and M. A. Goñi, 2003: Constancy in the vegetation of the Amazon basin during the late Pleistocene: Evidence from the organic matter composition of Amazon deep fan sediments. *Geology*, **31**, 291-294.

Kleidon, A., and S. Lorenz, 2001: Deep roots sustain Amazonian rainforest in climate model simulations of the last ice age. *Geophys. Res. Lett.* **28**, 2425–2428.

Knapp, S., and J. Mallet, 2003: Refuting refugia? *Science*, **300**, 71-72.

Lenters, J.D., and K.H.Cook, 1995: Simulation and diagnosis of the regional South American precipitation climatology. *J. Climate*, **8**, 2988-3005.

Li, W., R. Fu, and R.E. Dickinson, 2006: Rainfall and its seasonality over the Amazon in the 21st century as assessed by the coupled models for the IPCC AR4. J. Geophys. Res., 111, D02111, doi:10.1029/2005JD006355.

Malhi, Y., and J. Wright, 2004: Spatial patterns and recent trends in the climate of tropical rainforest regions. *Phil. Trans. Roy. Meteorol. Soc*., **359**, 311-329.

Mayle, F. E., D. J. Beerling, W. D. Gosling, and M. B. Bush, 2004: Responses of Amazonian ecosystems to climatic and atmospheric carbon dioxide changes since the last glacial maximum. *Philos. Trans. of the Roy. Soc. of London, Series B-Biol. Sci*. 359, 499-514.

Menendez, C.G., 2005: Ensemble mean large-scale r response over South America from IPCC AR4 models. *CLARIS News*, **3**, 21 – 24.

Mitas, C.M., and A. Clement, 2005: Has the Hadlet cell been strengthening in recent decades? Geophys. Res. Letters, 32 (3): Art. No. L030809.

New, M., D. Lister, M. Hulme, and I. Makin, 2000: A high-resolution data set of surface climate over global land areas. *Climate Res.*, **21**, 1-25.

Oyama, M.D., and C. A. Nobre, 2004: A simple potential vegetation model for coupling with the Simple Biosphere Model. Brazilian Journal of Meteorology, 19, 204-216.

Prentice, I.C., W. Cramer, S.P. Harrison, et al., 1992 : A global biome model based on plant physiology and dominance, soil properties, and climate. *J. Biogeog*., **19**, 117-134.

Rojas, M., A. Seth, and S.A. Rauscher, 2006: Relationship between precipitation and moisture flux changes in the SRES A2 scenario for the South American monsoon region. *CLARIS News*, **3**, 14 – 20.

Scholze, M., W. Knorr, N.W. Arnell, and I.C. Prentice, 2006: A climate-change risk analysis for world ecosystems. *Proc. of the Nat. Acad. Sci*., **103**, 13116-13120.

Tanaka, H.L., N. Ishizaki, and A. Kitoh, 2004: Trend and interannual variability of Walker, monsoon and Hadley circulations defined by velocity potential in the upper troposphere. *Tellus-A*, **56**, 250-269.

Vecchi, G.A., B.J. Soden, A. T. Wittenberg, I. M. Held, A. Leetmaa, and M. J. Harrison, 2006: Weakening of tropical Pacific atmospheric circulation due to anthropogenic forcing. *Nature*, **441**, 73-76.

Vecchi, G.A., and B.J. Soden, 2007: Global warming and the weakening of the tropical circulation. *J. Climate*, in press.

Vera, C., G. Silvestri, B. Liebmann, and P. Gonzalez, 2006*:* Climate change scenarios for seasonal precipitation in South America from IPCC-AR4 models. *Geophys. Res. Lett.,* **33**, 13, doi:10.1029/2006GL025759.

Vizy, E. K., and K. H. Cook, 2005: Evaluation of Last Glacial Maximum sea surface temperature reconstructions through their influence on South American climate, J. Geophys. Res., 110, D11105, doi:10.1029/2004JD005415.

Vizy, E.K., and K.H., Cook, 2007: Relationship between Amazon and high Andes precipitation. *J. Geophysical Research – Atmospheres*, **112** (D7): Art. No. D07107.

Woodward, F.I., 1987: *Climate and Plant Distribution*. Cambridge University Press. 174 pp.

Xie, P., and P. A. Arkin, 1997: Global precipitation: A 17-year monthly analysis based on gauge observations, satellite estimates, and numerical model outputs. *Bull. Amer. Meteorol. Soc.*, **78**, 2539-2558.

Xue Y., F. de Sales, W.P. Li, et al., 2006: Role of land surface processes in South American monsoon development. J. Cli., 19, 741-762.

Zhang, M. and H. Song, 2006: Evidence of deceleration of atmospheric vertical overturning circulation over the tropical Pacific, *Geophys. Res. Lett.*, **33**, L12701, doi:/10.1029/2006GL025942.

Figure captions

Table 1. Simulations with the coupled RCM/PVM.

Figure 1. Schematic of the asynchronous coupling method used for communication between the regional climate model (RCM) and the potential vegetation model (PVM).

Figure 2. Annual mean precipitation in mm/day from the (a) CRU 10-minute 1961-1990 (land) and CPC (ocean) climatologies, (b) the CCCMA 20th century GCM integration (1981-2000), and the regional model simulations (c) Present_CCC and (d) Present_Reanalysis.

Figure 3. (a) Observed vegetation distribution over South America from the USGS. Vegetation distribution in equilibrium with the (b) CCCMA 1981-2000 climatology, (c) RCM constrained by lateral boundary conditions from the 1981-2000 CCCMA climatology and (d) RCM constrained by lateral boundary conditions from the 1981-2000 NCEP/NCAR reanalysis climatology. The numbers indicate standard USGS vegetation categories as follows: 1 = cropland, 2 = grassland, 3 = shrubland and mixed shrubland/grassland (caatinga), 4 = savanna, 5 = deciduous forest, 6 = evergreen (rain) forest, 7 = barren or sparsely vegetated, 8 = tundra. (A few USGS vegetation categories are combined in the figure to make the display clearer.)

Figure 4. Vegetation distribution for (a) 1981-2000 from the Present_Coupled simulation and for (b) 2080-2100 from the Future_Coupled simulation (see Table 1). Shading and numbering of vegetation categories as in Figure 3.

Figure 5. Shading denotes regions with annual precipitation too low to support rainforest vegetation rainforest in the (a) present day and (b) 2080-2100 climatology simulated by the coupled RCM/PVM. In (c) and (d), shading indicates regions unsuitable for rainforest vegetation because the dry season is too long in the (c) present day and (d) 2080-2100

climatology simulated by the coupled RCM/PVM model. The contour in (c) and (d) superimposes the boundary from (a) and (b).

Figure 6. Shaded regions are those in which the wetness criterion, H, is low enough to allow for the presence of caatinga vegetation in the (a) present day simulation and (b) 2080-2100 climatology simulated by the coupled RCM/PVM model. In (c) and (d), shading denotes regions suitable for caatinga vegetation according to the seasonality criterion, D, in the (c) present day and (d) 2080-2100 simulations. The contour in (c) and (d) superimposes the wetness criterion boundary from (a) and (b).

Figure 7. Differences in annual precipitation, with boxes to indicate regions used for averaging. The heavy line is the 0 mm/day contour, the contour interval is 2 mm/day, and lighter shading indicates negative values.

Figure 8. Monthly mean precipitation in mm/day in each region denoted in Figure 7 for the present day (1981-2000; solid line) and 2081-2100 (dashed line) simulations. Note that the y-axis scales differ.

Figure 9. Simulated 900 hPa geopotential heights (shading and contours) and moisture transport in January for (a) 1981-2000, (b) 2081-2100, and (c) their difference (future – present day). Simulated geopotential heights and moisture transport at 900 hPa in March for (d) 1981-2000, (e) 2081-2100, and (f) their difference (future – present day). Vector scale is in $(kg - H_2O / kg - air)(m/s)$, and the geopotential height contour interval is 10 gpm.

Figure 10. Simulated 900 hPa geopotential heights (shading and contours) and moisture transport in August for (a) 1981-2000, (b) 2081-2100, and (c) their difference (future – present day). Simulated geopotential heights and moisture transport at 900 hPa in September for (d) 1981-2000, (e) 2081-2100, and (f) their difference (future – present day). Vector scale is in $(kg - H_2O / kg - air)(m/s)$, and the geopotential height contour interval is 10 gpm.

Figure 11. Simulated South American vegetation distribution in 2081-2100 for the (a) first and (b) second iteration of the coupled RCM/PVM model. Vegetation type is indicated by shading and numbers as in Fig. 3.

Table 1. Simulations with the coupled RCM/PVM.

Simulation	SSTs	Land Surface	Atmospheric CO_2	Boundary Conditions
Present_Reanalysis	Shea et al. (1992)	present day from USGS	330 ppmv	1981-2000 reanalysis
Present_CCC	1981-2000 CCCMA climatology	present day from USGS	330 ppmv	1981-2000 CCCMA 20C3M climatology
Present_Coupled	Shea et al. (1992)	1 iteration from present day vegetation	330 ppmv	1981-2000 reanalysis
Future_Coupled	Shea et al. (1992) SSTs + CCC SRESA2 anomalies	3 iterations from present day vegetation	757 ppmv	reanalysis climatology + CCCMA SRESA2 anomalies
CO_2-Alone	Shea et al. (1992)	present day from USGS	757 ppmv	1981-2000 reanalysis
SST-Alone	Shea et al. (1992) SSTs + CCC SRESA2 anomalies	present day from USGS	330 ppmv	1981-2000 reanalysis
Lateral-Alone	Shea et al. (1992)	present day from USGS	330 ppmv	reanalysis climatology + CCCMA SRESA2 anomalies

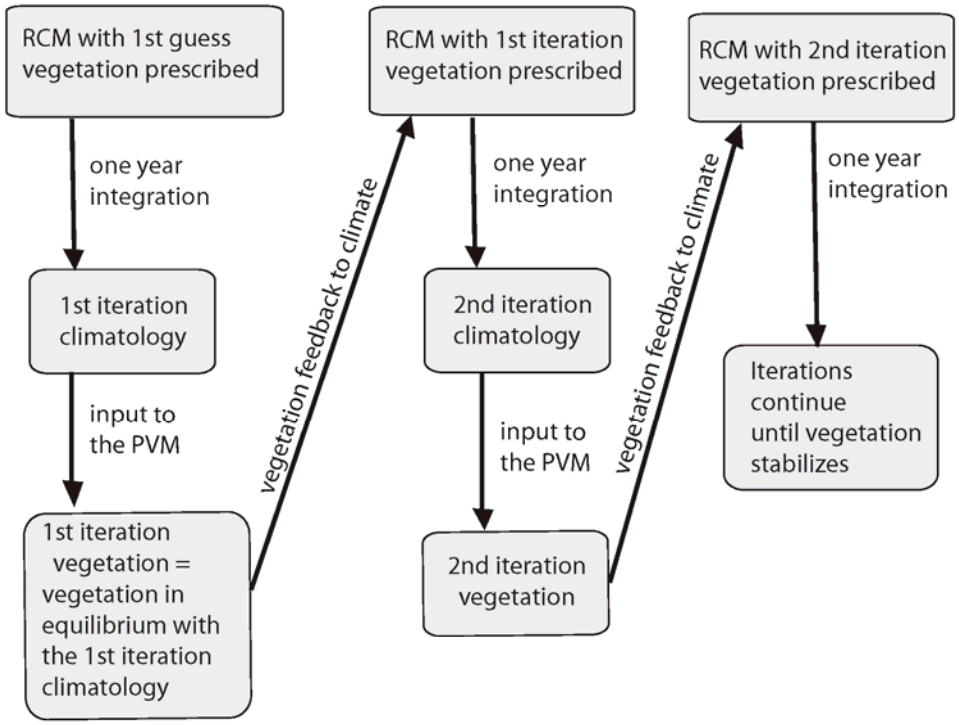

Figure 1. Schematic of the asynchronous coupling method used for communication between the regional climate model (RCM) and the potential vegetation model (PVM).

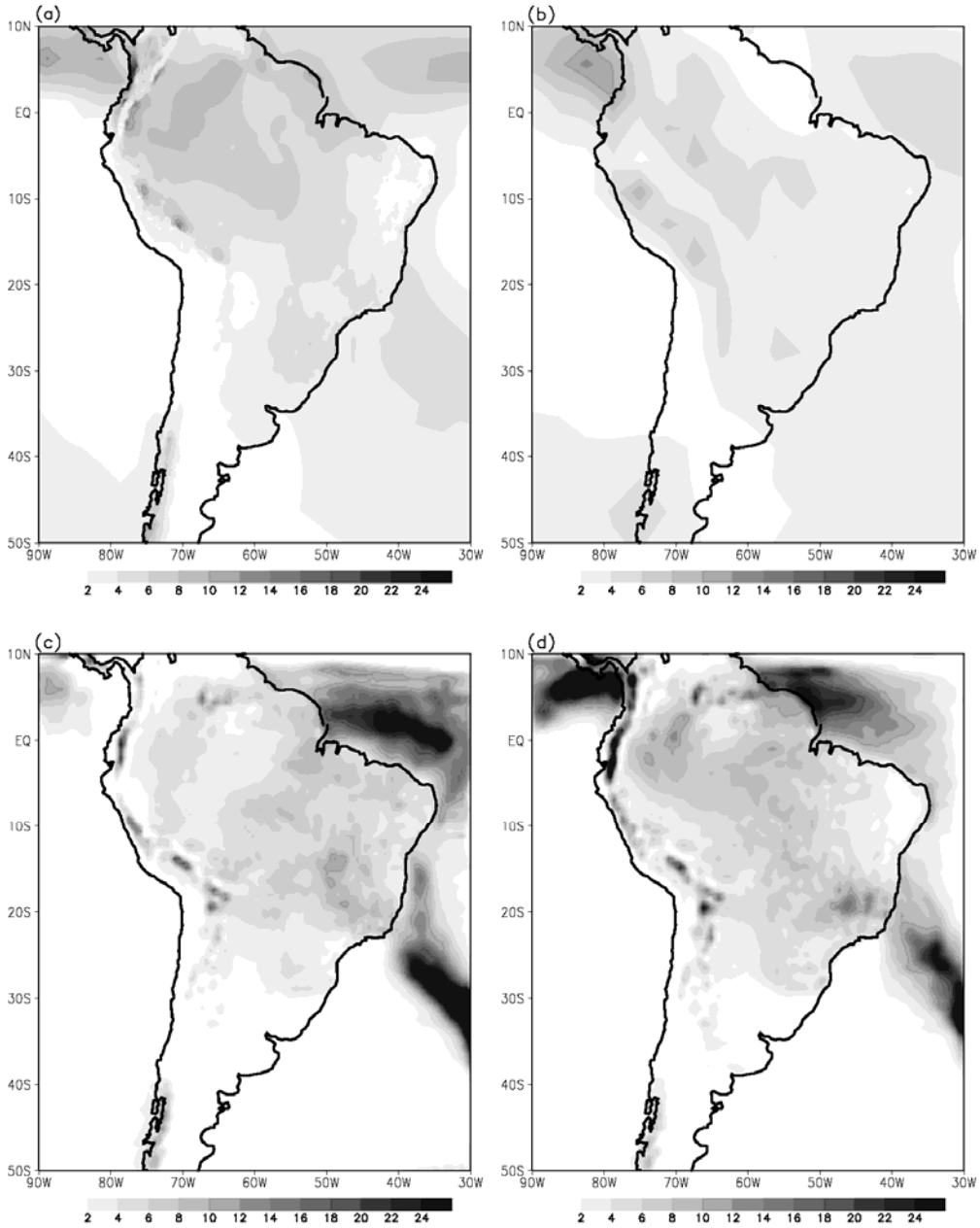

Figure 2. Annual mean precipitation in mm/day from the (a) CRU 10-minute 1961-1990 (land) and CPC (ocean) climatologies, (b) the CCCMA 20th century GCM integration (1981-2000), and the regional model simulations (c) Present_CCC and (d) Present_Reanalysis.

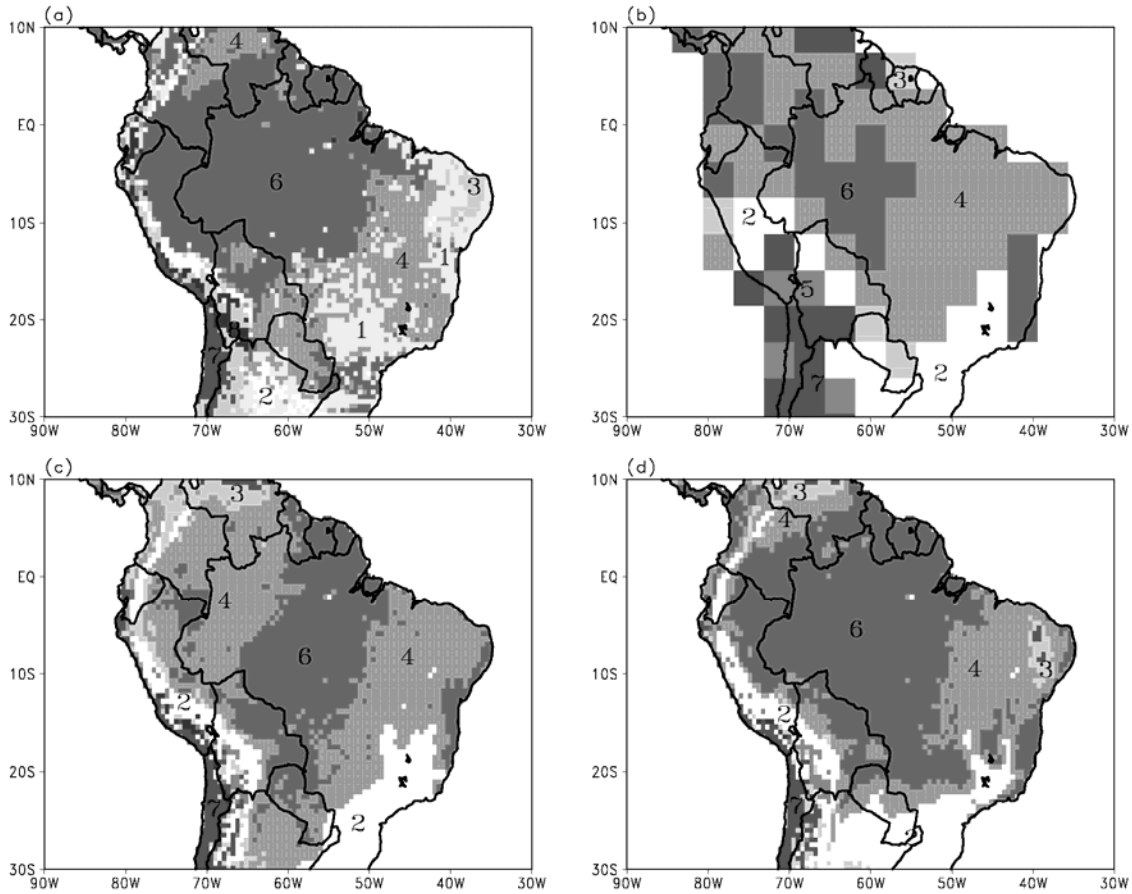

Figure 3. (a) Observed vegetation distribution over South America from the USGS. Vegetation distribution in equilibrium with the (b) CCCMA 1981-2000 climatology, (c) RCM constrained by lateral boundary conditions from the 1981-2000 CCCMA climatology and (d) RCM constrained by lateral boundary conditions from the 1981-2000 NCEP/NCAR reanalysis climatology. The numbers indicate standard USGS vegetation categories as follows: 1 = cropland, 2 = grassland, 3 = shrubland and mixed shrubland/grassland (caatinga), 4 = savanna, 5 = deciduous forest, 6 = evergreen (rain) forest, 7 = barren or sparsely vegetated, 8 = tundra. (A few USGS vegetation categories are combined in the figure to make the display clearer.)

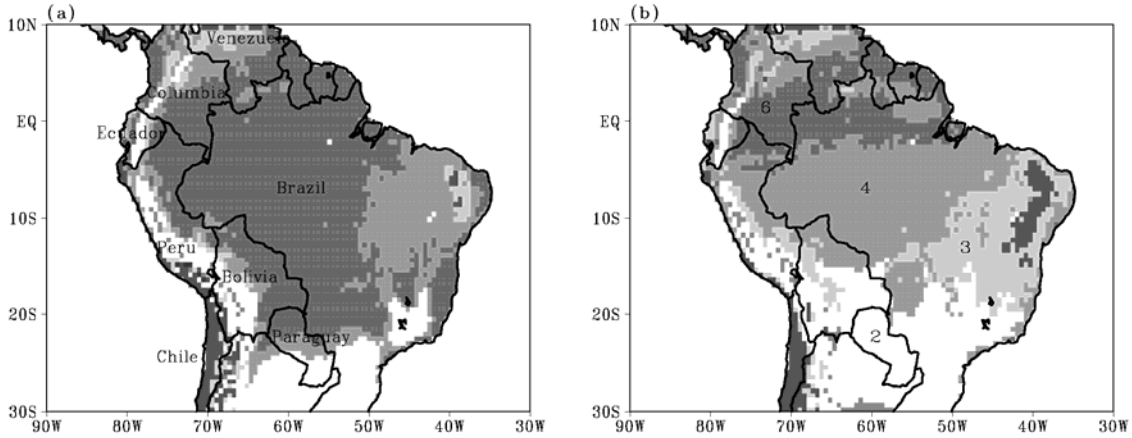

Figure 4. Vegetation distribution for (a) 1981-2000 from the Present_Coupled simulation and for (b) 2080-2100 from the Future_Coupled simulation (see Table 1). Shading and numbering of vegetation categories as in Figure 3.

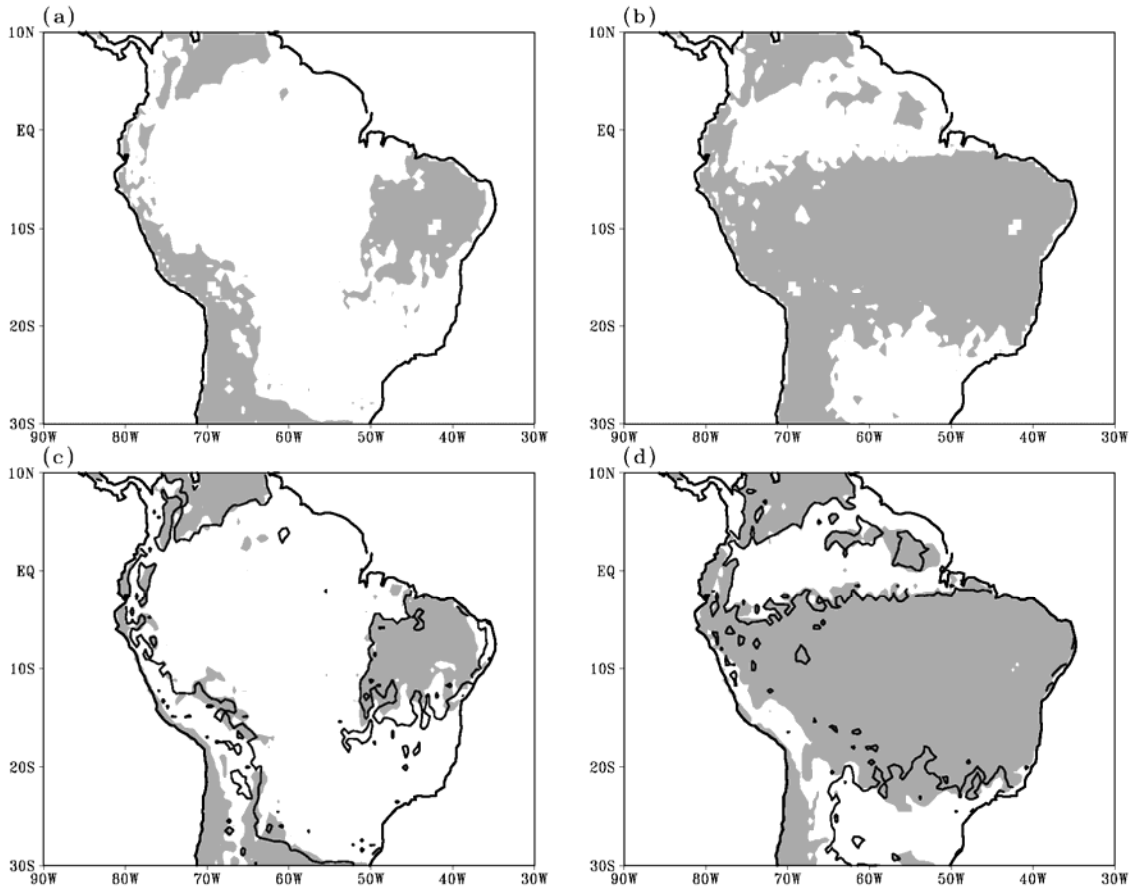

Figure 5. Shading denotes regions with annual precipitation too low to support rainforest vegetation rainforest in the (a) present day and (b) 2080-2100 climatology simulated by the coupled RCM/PVM. In (c) and (d), shading indicates regions unsuitable for rainforest vegetation because the dry season is too long in the (c) present day and (d) 2080-2100 climatology simulated by the coupled RCM/PVM model. The contour in (c) and (d) superimposes the boundary from (a) and (b).

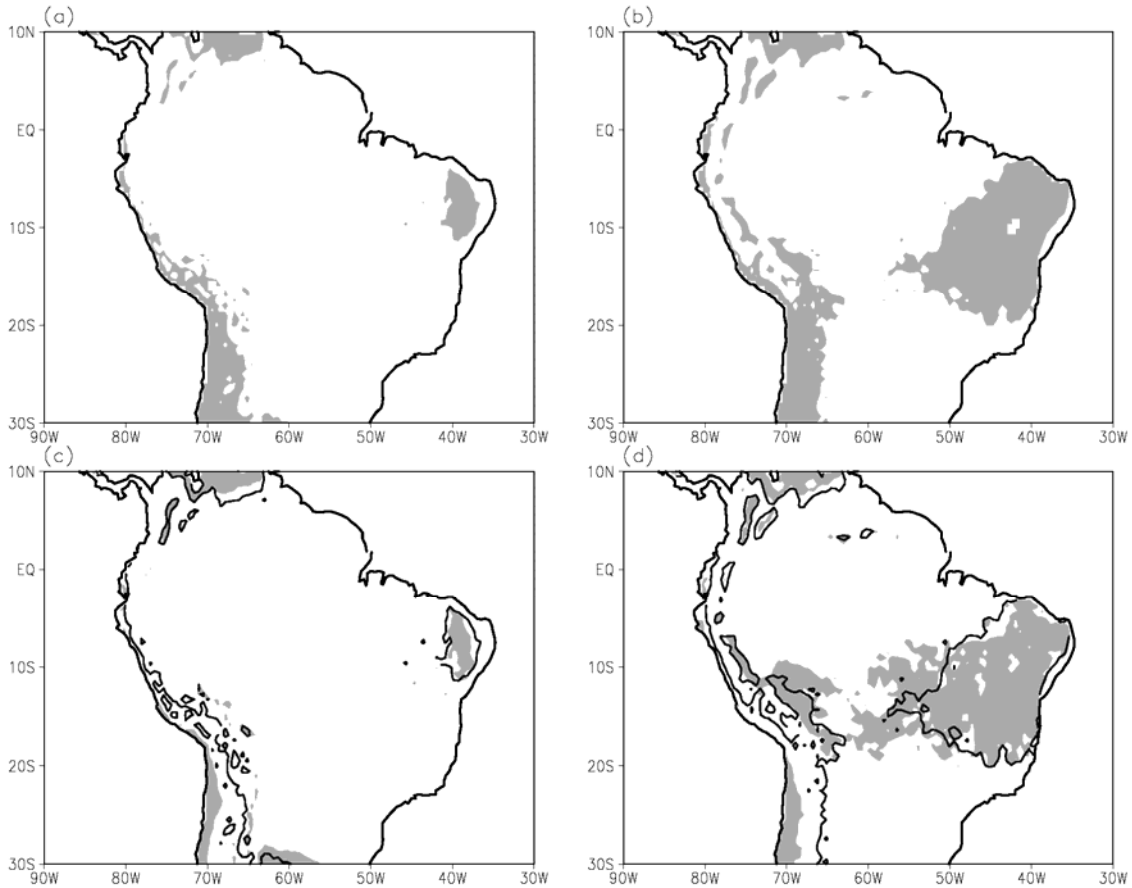

Figure 6. Shaded regions are those in which the wetness criterion, H, is low enough to allow for the presence of caatinga vegetation in the (a) present day simulation and (b) 2080-2100 climatology simulated by the coupled RCM/PVM model. In (c) and (d), shading denotes regions suitable for caatinga vegetation according to the seasonality criterion, D, in the (c) present day and (d) 2080-2100 simulations. The contour in (c) and (d) superimposes the wetness criterion boundary from (a) and (b).

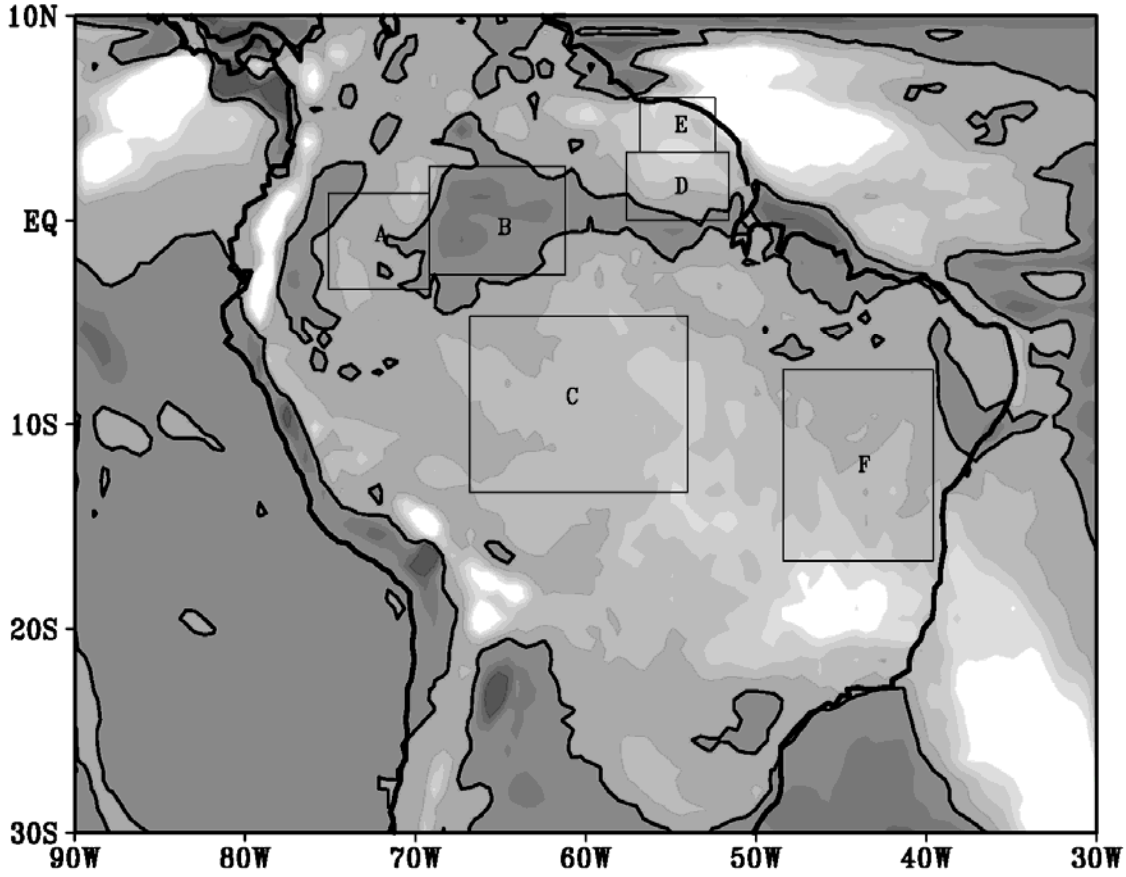

Figure 7. Differences in annual precipitation, with boxes to indicate regions used for averaging. The heavy line is the 0 mm/day contour, the contour interval is 2 mm/day, and lighter shading indicates negative values.

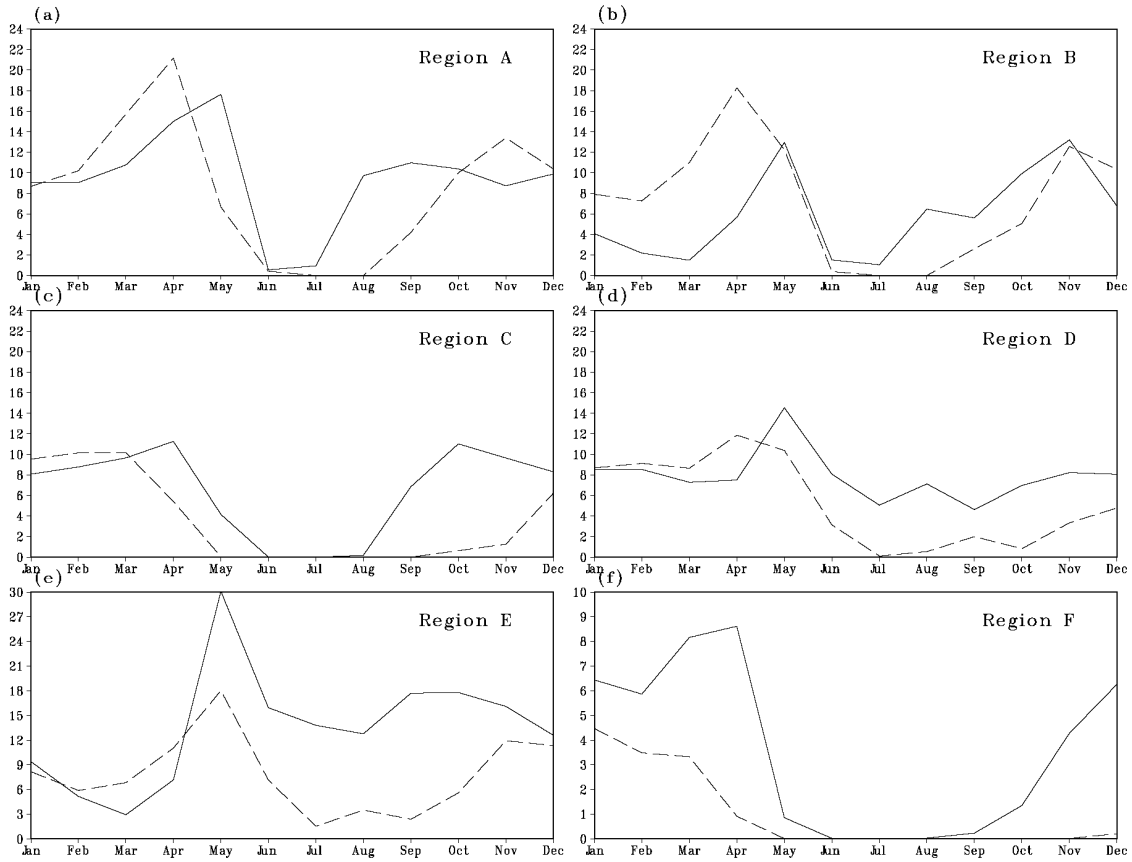

Figure 8. Monthly mean precipitation in mm/day in each region denoted in Figure 7 for the present day (1981-2000; solid line) and 2081-2100 (dashed line) simulations. Note that the y-axis scales differ.

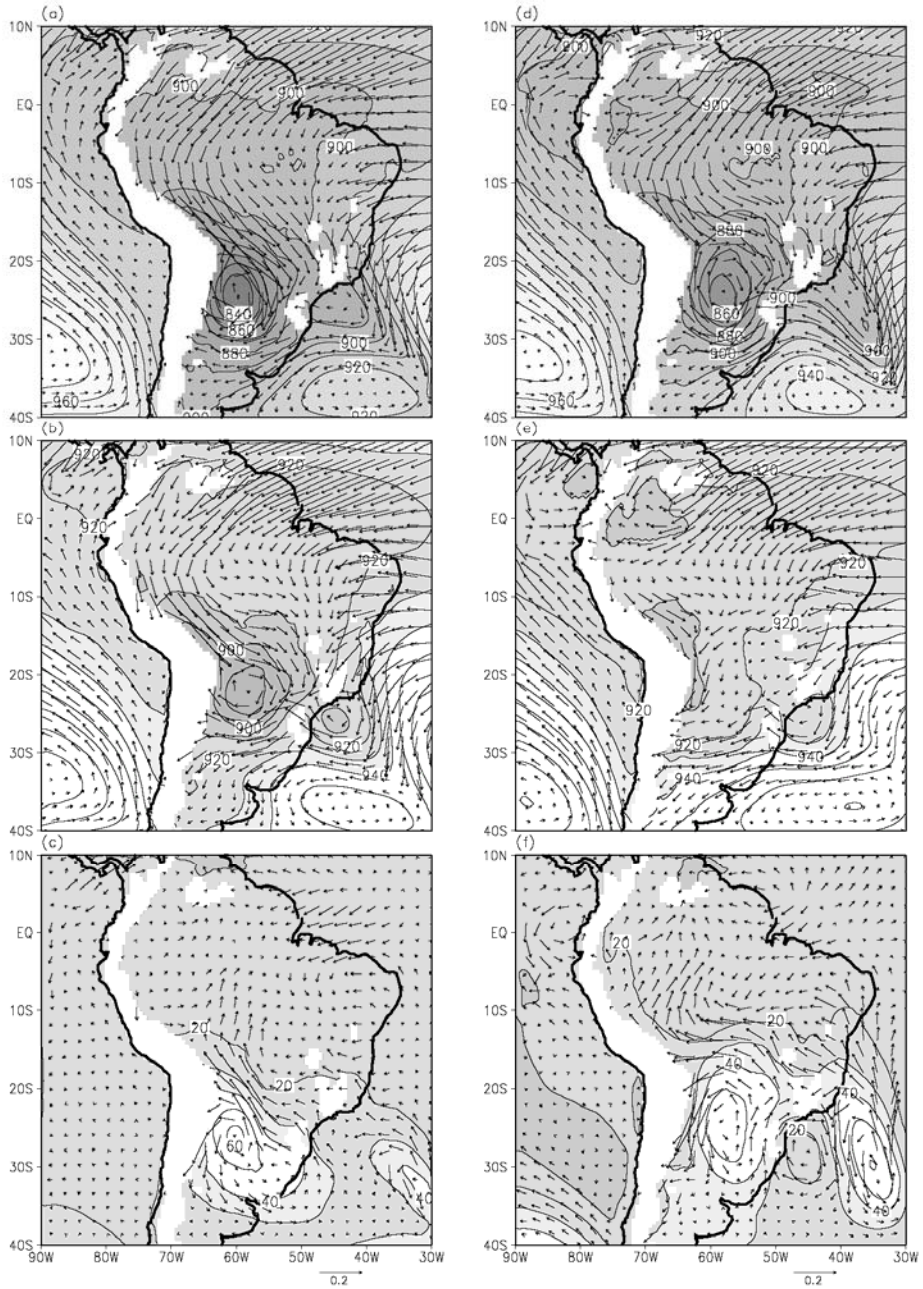

Figure 9. Simulated 900 hPa geopotential heights (shading and contours) and moisture transport in January for (a) 1981-2000, (b) 2081-2100, and (c) their difference (future – present day). Simulated geopotential heights and moisture transport at 900 hPa in March for (d) 1981-2000, (e) 2081-2100, and (f) their difference (future – present day). Vector scale is in $\left(kg-H_2O/kg-air\right)\left(m/s\right)$, and the geopotential height contour interval is 10 gpm.

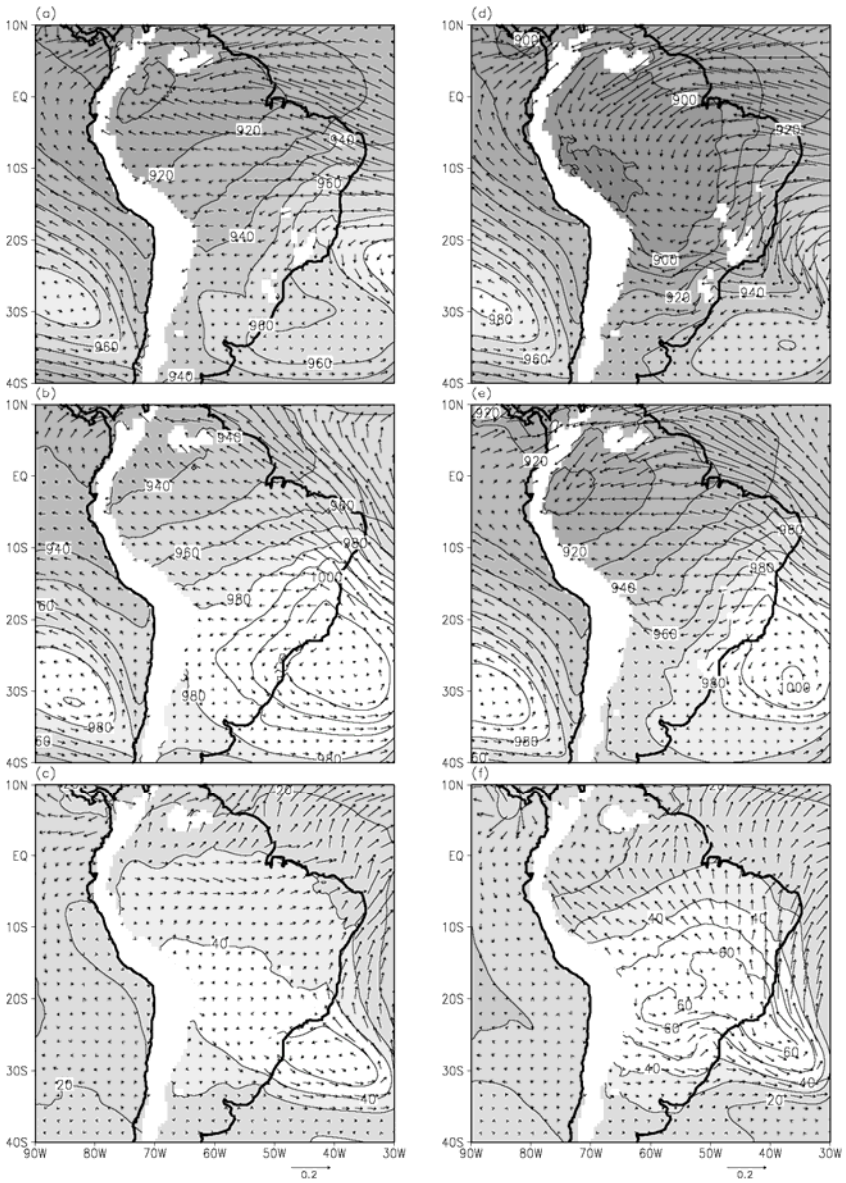

Figure 10. Simulated 900 hPa geopotential heights (shading and contours) and moisture transport in August for (a) 1981-2000, (b) 2081-2100, and (c) their difference (future – present day). Simulated geopotential heights and moisture transport at 900 hPa in September for (d) 1981-2000, (e) 2081-2100, and (f) their difference (future – present day). Vector scale is in $\left(kg - H_2O / kg - air\right)\left(m / s\right)$, and the geopotential height contour interval is 10 gpm.

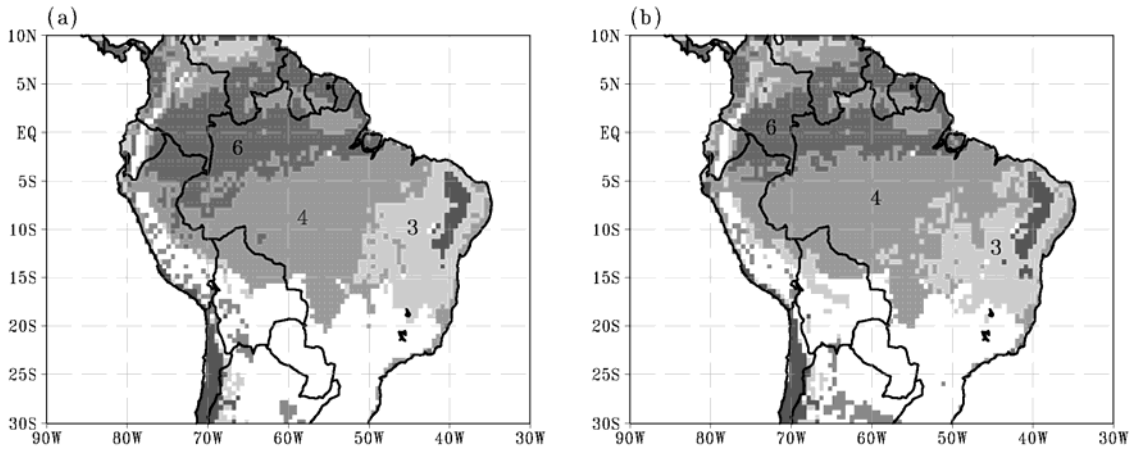

Figure 11. Simulated South American vegetation distribution in 2081-2100 for the (a) first and (b) second iteration of the coupled RCM/PVM model. Vegetation type is indicated by shading and numbers as in Fig. 3.